

The forward problem algorithm based on modified element free Galerkin method for bioluminescence tomography

Chenghu Qin, Jie Tian*, *Senior member, IEEE*, Kai Liu and Yakang Dai

Abstract—As an emerging and promising molecular imaging modality, bioluminescence tomography (BLT) can reconstruct the internal light source with the photon fluence on the small animal surface to reveal non-invasive molecular and cellular activities directly. In order to obtain higher precision and better spatial resolution in source reconstruction, the solution accuracy for the forward problem of BLT should be improved as high as possible. In this contribution, we present a modified element free Galerkin method (MEFGM) to calculate photon propagation in the biological tissue. This method is based on moving least squares (MLS) approximation which requires only a series of nodes in the region of interest, so complicated meshing task can be avoided compared with finite element method (FEM). Furthermore, MLS shape functions are further modified to satisfy the delta function property, which can simplify the processing of boundary conditions in comparison with traditional meshless methods. Finally, the numerical simulation experiments demonstrate the effectiveness and feasibility of this proposed method by comparing the solution of MEFGM with that of FEM.

I. INTRODUCTION

Small animal molecular imaging has been rapidly developed and applied to biomedical research over the past years [1]. As a new optical molecular imaging modality, bioluminescence tomography (BLT) has become an effective approach for *in vivo* imaging because it not only can reveal *in vivo* cellular and molecular processes selectively and directly, but also has high sensitivity and cost-effectiveness in comparison with other imaging techniques [2], [3], [4]. The goal of BLT is to reconstruct the internal bioluminescent source with the measured bioluminescent signal on the external surface of a living small animal, which can be used for tumorigenesis studies, cancer diagnosis, gene therapies, metastasis detection, drug discovery and development *etc.* The forward problem of BLT, which describes light transport in tissue, is employed not only to predict the distribution of the bioluminescent light on the object surface, but also to generate a sensitive matrix that relates the measurements to the internal optical properties and will be used in the inverse problem [5]. Therefore, the accuracy improvement of numerical solution to the forward problem of BLT is favorable to enhance localization and quantification of the reconstructed bioluminescent source.

This work is supported by NBRPC (2006CB705700), PCSIRT (IRT0645), CAS HTP, CAS SREDP (YZ0642, YZ200766), 863 Program (2006AA04Z216), JRFOYS (30528027), NSFC (30672690, 30600151, 30500131 and 60532050), BNSF (4071003) in China.

C. Qin, J. Tian, K. Liu and Y. Dai are with Medical Image Processing Group, Key Laboratory of Complex Systems and Intelligence Science, Institute of Automation, Chinese Academy of Sciences. e-mail: tian@ieee.org

In bio-photonics, the diffusion equation has been commonly used to model photon propagation in the biological tissue because the radiative transfer equation (RTE) is extremely computationally expensive for its integro-differential nature [3], [5]. As we all know, analytical, statistical and numerical techniques are three kinds of methods to solve the aforementioned diffusion equation [5]. Among these methods, numerical techniques are studied widely for high efficiency and good applicability, and finite element method (FEM) is one of the most typical and successful algorithms. However, mesh generation and data pre-processing for FEM is difficult and time-consuming, especially for three dimensional irregular objects with complex internal structure [5]. In this paper, a modified element free Galerkin method (MEFGM) is developed to solve the forward problem of BLT firstly. Compared with FEM, MEFGM uses only a series of nodes and does not require node connectivity or element data, which helps not only to avoid burdensome meshing but also to describe complex inhomogeneous domains more accurately [6]. Furthermore, the good accuracy and high convergence rate of meshless methods have been proved, and post-processing of calculation results is very simple [7], [8]. In addition, *a priori* knowledge of the tissue optical parameters should be incorporated in our algorithm, which can be obtained from optical database or diffuse optical tomography (DOT) [9].

The paper is organized as follows. The next section introduces the proposed MEFGM algorithm for the forward problem of BLT. In section 3, the performance of this method is tested using square and cubic phantoms and compared with the simulation results by FEM. Finally, the conclusion and future work are provided.

II. METHOD

A. Diffusion approximation and boundary condition

In bioluminescence imaging, the propagation of bioluminescent photons in the biological tissue can be depicted by steady-state diffusion equation because photon scattering dominates over absorption [3], [10], [11]:

$$-\nabla \cdot (D(\mathbf{x})\nabla\Phi(\mathbf{x})) + \mu_a(\mathbf{x})\Phi(\mathbf{x}) = S(\mathbf{x}) \quad (\mathbf{x} \in \Omega) \quad (1)$$

where Ω is the given domain; $\Phi(\mathbf{x})$ represents the photon flux density [*Watts/mm²*]; $S(\mathbf{x})$ denotes the bioluminescent source density [*Watts/mm³*]; $\mu_a(\mathbf{x})$ is the absorption coefficient [*mm⁻¹*]; $D(\mathbf{x}) = (3(\mu_a(\mathbf{x}) + (1-g)\mu_s(\mathbf{x})))^{-1}$ is the optical diffusion coefficient, $\mu_s(\mathbf{x})$ the scattering coefficient [*mm⁻¹*] and g the anisotropy parameter.

When the bioluminescence imaging experiment is carried out in a totally dark environment, the boundary condition can be expressed as:

$$\Phi(\mathbf{x}) + 2A(\mathbf{x}; n, n')D(\mathbf{x})(\mathbf{v}(\mathbf{x}) \cdot \nabla \Phi(\mathbf{x})) = 0 \quad (\mathbf{x} \in \partial\Omega) \quad (2)$$

where $\partial\Omega$ is the boundary of Ω ; $\mathbf{v}(\mathbf{x})$ is the unit outer normal on $\partial\Omega$; $A(\mathbf{x}; n, n')$ is a function to incorporate the mismatch between the refractive indices n within Ω and n' in the surrounding medium. In our study, the measured outgoing flux density $Q(\mathbf{x})$ on $\partial\Omega$ is:

$$Q(\mathbf{x}) = -D(\mathbf{x})(\mathbf{v} \cdot \nabla \Phi(\mathbf{x})) = \frac{\Phi(\mathbf{x})}{2A(\mathbf{x}; n, n')} \quad (\mathbf{x} \in \partial\Omega) \quad (3)$$

B. Modified element free Galerkin method

1) *Moving least squares approximation:* Moving least squares (MLS) approximation is the basis of MEFGM. According to the literatures [7] and [8], $\Phi(\mathbf{x})$ can be approximated by $\Phi^h(\mathbf{x})$ in the given domain Ω :

$$\Phi(\mathbf{x}) \approx \Phi^h(\mathbf{x}) = \sum_{j=1}^m p_j(\mathbf{x})a_j(\mathbf{x}) = \mathbf{p}^T(\mathbf{x})\mathbf{a}(\mathbf{x}) \quad (4)$$

where $p_j(\mathbf{x})$ is the monomial basis function, and m is the number of the basis functions; $a_j(\mathbf{x})$ is the non-constant coefficient which can be obtained by minimizing the following weighted quadratic functional $J(\mathbf{x})$:

$$J(\mathbf{x}) = \sum_{i=1}^{N_n} w(\mathbf{x} - \mathbf{x}_i) [\mathbf{p}^T(\mathbf{x}_i)\mathbf{a}(\mathbf{x}) - \Phi_i]^2 \quad (5)$$

where N_n is the number of nodes in Ω ; $w(\mathbf{x} - \mathbf{x}_i)$ denotes the weight function related to the node \mathbf{x} , and \mathbf{x}_i is a node in the support domain of \mathbf{x} for which $w(\mathbf{x} - \mathbf{x}_i) \neq 0$.

After the minimization of $J(\mathbf{x})$, the following linear equation can be obtained:

$$\mathbf{A}(\mathbf{x})\mathbf{a}(\mathbf{x}) = \mathbf{B}(\mathbf{x})\Phi \quad (6)$$

where

$$\mathbf{A}(\mathbf{x}) = \sum_{i=1}^{N_n} w(\mathbf{x} - \mathbf{x}_i)\mathbf{p}(\mathbf{x}_i)\mathbf{p}^T(\mathbf{x}_i) \quad (7)$$

$$\mathbf{B}(\mathbf{x}) = [w(\mathbf{x} - \mathbf{x}_1)\mathbf{p}(\mathbf{x}_1), \dots, w(\mathbf{x} - \mathbf{x}_{N_n})\mathbf{p}(\mathbf{x}_{N_n})] \quad (8)$$

$$\Phi = (\Phi_1, \Phi_2, \dots, \Phi_{N_n})^T \quad (9)$$

Solving $\mathbf{a}(\mathbf{x})$ from Eq. (6) and inserting it into Eq. (4), we can obtain the following MLS approximation form:

$$\Phi^h(\mathbf{x}) = \sum_{i=1}^{N_n} N_i(\mathbf{x})\Phi_i \quad (10)$$

where the shape function $N_i(\mathbf{x})$ is defined by

$$N_i(\mathbf{x}) = \mathbf{p}^T(\mathbf{x})\mathbf{A}^{-1}(\mathbf{x})\mathbf{B}_i(\mathbf{x}) \quad (11)$$

where $\mathbf{B}_i(\mathbf{x})$ stands for the i th column of the matrix $\mathbf{B}(\mathbf{x})$.

The partial derivatives of the shape function $N_i(\mathbf{x})$ are given by

$$N_{i,s}(\mathbf{x}) = \mathbf{p}_{,s}^T \mathbf{A}^{-1} \mathbf{B}_i + \mathbf{p}^T [\mathbf{A}^{-1} (\mathbf{B}_{i,s} - \mathbf{A}_{,s} \mathbf{A}^{-1} \mathbf{B}_i)] \quad (12)$$

where s represents a spatial variable.

In this contribution, the linear basis function

$$\mathbf{p}^T(\mathbf{x}) = [1, x, y, z], \quad m = 4 \quad (13)$$

and the following cubic spline weight function are used in the three dimensional case.

$$w(r) = \begin{cases} 2/3 - 4r_i^2 + 4r_i^3 & r_i \leq 1/2 \\ 4/3 - 4r_i + 4r_i^2 - 4r_i^3/3 & 1/2 < r_i \leq 1 \\ 0 & r_i > 1 \end{cases} \quad (14)$$

where $r_i = \|\mathbf{x} - \mathbf{x}_i\|/d^{max}$ is the ratio of the Euclidean distance between the evaluation point \mathbf{x} and the node \mathbf{x}_i to the radius of the support domain d^{max} .

2) *Modified MLS shape function:* Substituting $\mathbf{x} = \mathbf{x}_k$ back into Eq. (10), we have

$$\Phi^h(\mathbf{x}_k) = \sum_{i=1}^{N_n} N_i(\mathbf{x}_k)\Phi_i = \mathbf{N}_k^T \Phi \quad (15)$$

where Φ represents the generalized photon flux density, and $\mathbf{N}_k = [N_1(\mathbf{x}_k), N_2(\mathbf{x}_k), \dots, N_{N_n}(\mathbf{x}_k)]^T$. Then, Eq. (15) can be further written as the following matrix equation:

$$\hat{\Phi} = \mathbf{\Lambda}^T \Phi \quad (16)$$

where $\hat{\Phi}$ denotes the nodal photon flux density, and $\mathbf{\Lambda}$ is referred to as full transformation matrix. They can be expressed as:

$$\hat{\Phi} = [\Phi^h(\mathbf{x}_1), \Phi^h(\mathbf{x}_2), \dots, \Phi^h(\mathbf{x}_{N_n})]^T \quad (17)$$

$$\mathbf{\Lambda} = \begin{bmatrix} N_1(\mathbf{x}_1) & N_1(\mathbf{x}_2) & \dots & N_1(\mathbf{x}_{N_n}) \\ N_2(\mathbf{x}_1) & N_2(\mathbf{x}_2) & \dots & N_2(\mathbf{x}_{N_n}) \\ \vdots & \vdots & \ddots & \vdots \\ N_{N_n}(\mathbf{x}_1) & N_{N_n}(\mathbf{x}_2) & \dots & N_{N_n}(\mathbf{x}_{N_n}) \end{bmatrix} \quad (18)$$

Therefore, the generalized photon flux density can be obtained from Eq. (16)

$$\Phi = \mathbf{\Lambda}^{-T} \hat{\Phi} \quad (19)$$

and

$$\Phi_i = \sum_{l=1}^{N_n} N_l(\mathbf{x}_i)^{-1} \hat{\Phi}_l \quad (20)$$

where $\mathbf{\Lambda}^{-1}$ is the inverse matrix of $\mathbf{\Lambda}$. Incorporating Eq. (20) with Eq. (10), we have

$$\Phi^h(\mathbf{x}) = \sum_{i=1}^{N_n} N_i(\mathbf{x}) \sum_{l=1}^{N_n} N_l(\mathbf{x}_i)^{-1} \hat{\Phi}_l = \sum_{l=1}^{N_n} M_l(\mathbf{x}) \hat{\Phi}_l \quad (21)$$

where $M_l(\mathbf{x}) = \sum_{i=1}^{N_n} N_i(\mathbf{x})N_l(\mathbf{x}_i)^{-1}$ is called modified MLS shape function, and it satisfies the Kronecker delta function property:

$$M_l(\mathbf{x}_k) = \sum_{i=1}^{N_n} N_i(\mathbf{x}_k)N_l(\mathbf{x}_i)^{-1} = \delta_{lk} \quad (22)$$

3) *Numerical implementation of weak form*: Based on Galerkin method and Gauss theory, Eqs. (1) and (2) can be transformed to the following weak form [10]:

$$\int_{\Omega} \left(D(\mathbf{x}) (\nabla \Phi(\mathbf{x})) \cdot (\nabla \Psi(\mathbf{x})) + \mu_a(\mathbf{x}) \Phi(\mathbf{x}) \Psi(\mathbf{x}) \right) d\mathbf{x} + \int_{\partial\Omega} \frac{1}{2A(\mathbf{x}; n, n')} \Phi(\mathbf{x}) \Psi(\mathbf{x}) d\mathbf{x} = \int_{\Omega} S(\mathbf{x}) \Psi(\mathbf{x}) d\mathbf{x} \quad (23)$$

Substituting Eq. (21) into Eq. (23), the matrix form can be obtained as follows:

$$(\mathbf{K} + \mathbf{C} + \mathbf{F}) \widehat{\Phi} = \mathbf{G} \widehat{\Phi} = \mathbf{S} \quad (24)$$

where the components of the matrices \mathbf{K} , \mathbf{C} , \mathbf{F} and the vector \mathbf{S} are given by

$$\begin{cases} K_{kl} = \int_{\Omega} D(\mathbf{x}) (\nabla M_k(\mathbf{x})) \cdot (\nabla M_l(\mathbf{x})) d\Omega \\ C_{kl} = \int_{\Omega} \mu_a(\mathbf{x}) M_k(\mathbf{x}) M_l(\mathbf{x}) d\Omega \\ F_{kl} = \int_{\partial\Omega} M_k(\mathbf{x}) M_l(\mathbf{x}) / (2A(\mathbf{x}; n, n')) d\partial\Omega \\ S_k = \int_{\Omega} S(\mathbf{x}) M_k(\mathbf{x}) d\Omega \end{cases} \quad (25)$$

Since the matrix \mathbf{G} is symmetric and positive definite, $\widehat{\Phi}$ can be computed with the formula:

$$\widehat{\Phi} = \mathbf{G}^{-1} \mathbf{S} \quad (26)$$

III. EXPERIMENTS AND RESULTS

In numerical simulation experiments, square and cubic phantoms were designed to evaluate the performance of our MEFGM algorithm respectively. Furthermore, we compared the MEFGM computational results with the simulation data by FEM.

A. Square phantom experiment

A square phantom with 30mm side length was used in this experiment, and a square bioluminescent source of 1.0mm side length and $1.0\text{ nano} - \text{Watts}/\text{mm}^2$ power density was centered at $(15.0, 15.0)$, as shown in Fig. 1(a). The optical parameters described in the reference [9] were assigned to the square: $\mu_a = 0.035$, $\mu_s = 6.0$, $g = 0.9$ and $n = 1.37$, which were regarded as *a priori* knowledge in our algorithm. In MEFGM study, 31×31 uniform node distribution was arranged in the above square, which is also presented in Fig. 1(a). Finally, the bioluminescent photon flux density was solved using our MEFGM procedure, and Fig. 1(b) shows the corresponding computational result.

Besides, FEM was also employed to calculate the bioluminescent photon density in the square in order to demonstrate the accuracy of MEFGM. In FEM simulation, the square domain was discretized into 4609 nodes and 8928 triangular elements, as showed in Fig. 2(a), and then we used the interpolation method to compute the photon fluence at the points in MEFGM simulation. Fig. 2(b) gives the corresponding calculated photon fluence. The computational photon flux density based on MEFGM was in good agreement with the numerical result by FEM, with the average relative error being about 0.88% as presented in Fig. 3.

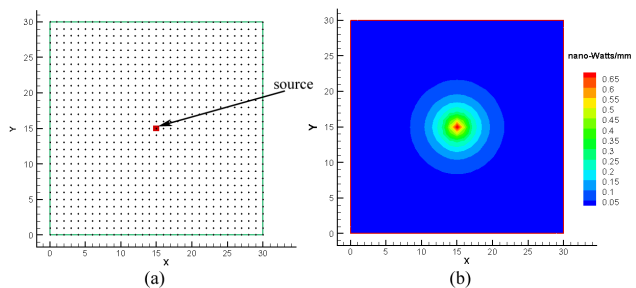


Fig. 1. Square phantom experiment. (a) The square domain with 31×31 uniform node distribution and a light source centered at $(15.0, 15.0)$; (b) The computational result using the MEFGM algorithm.

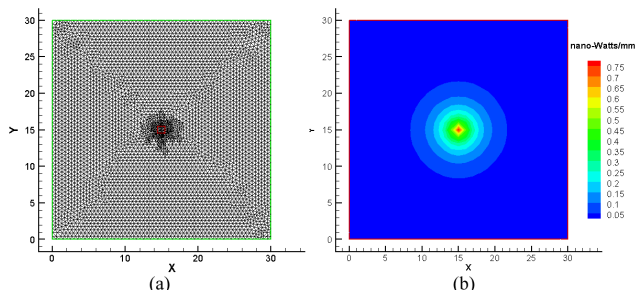


Fig. 2. (a) The discretized mesh used in FEM study; (b) The light exitance map solved by FEM.

B. Cubic phantom experiment

In order to further validate our MEFGM algorithm, a homogeneous cubic phantom with 20mm side length was set up. Meanwhile, a single cube light source of 1.0mm side length and $1.0\text{ nano} - \text{Watts}/\text{mm}^3$ power density was embedded into the phantom with its center at $(11.0, 11.0, 11.0)$, as showed in Fig. 4(a). The phantom optical parameters were also specified as: $\mu_a = 0.035$, $\mu_s = 6.0$, $g = 0.9$ and $n = 1.37$. We distributed $21 \times 21 \times 21$ nodes regularly in the cube. Finally, we obtained the bioluminescent light power on the surface of the phantom with the developed MEFGM algorithm, as presented in Fig. 4(b).

In addition, we also compared the above result with the simulation solution by FEM. First, we divided the cubic phantom into 15387 nodes and 81440 tetrahedral elements, as shown in Fig. 5(a). Fig. 5(b) is the surface light power distribution calculated by FEM. There is a good agreement between the solution of MEFGM and that of FEM with the average relative error being about 5.34%, as showed in Fig. 6. It is worth mentioning that all the computational results in this section have not been processed by any algorithm like normalization.

IV. CONCLUSION AND FUTURE WORK

Molecular imaging has been rapidly developed and used to study physiological and pathological processes *in vivo* at the cellular and molecular levels in recent years. Among molecular imaging techniques, BLT has become a research focus for its high signal-noise-ratio, low background noise

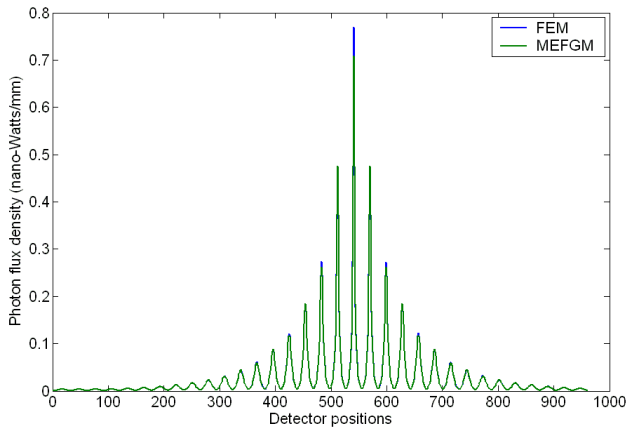


Fig. 3. Comparison between the solution of MEFGM and the result by FEM.

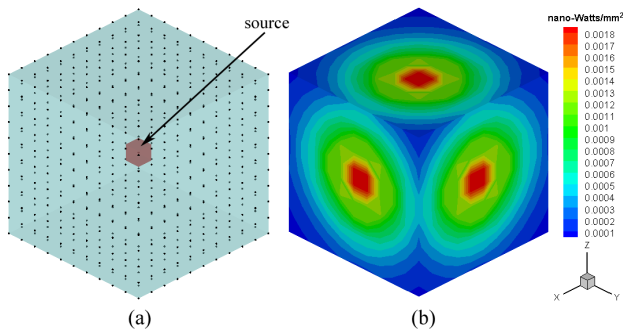


Fig. 4. Cubic phantom simulation. (a) A cubic phantom with a series of regularly arranged nodes and a light source; (b) The surface light power simulated by MEFGM.

and high sensitivity. The research of the forward problem of BLT is necessary because it helps not only to improve the precision and spatial resolution of source reconstruction but also to test the model of light transport in tissue. In this paper, we have presented a novel MEFGM algorithm to simulate the bioluminescent photon propagation in the biological tissue. In comparison with conventional FEM and boundary element method (BEM), the developed MEFGM algorithm uses only a group of nodes without consideration of element connectivity, so the troublesome mesh generation can be avoided. Furthermore, the post-processing is simple because the computational results have been already smooth. The numerical studies show that the MEFGM results and the FEM solution have the same tendency and good agreement.

Our future work will focus on employing the MEFGM algorithm to reconstruct the bioluminescent source. The corresponding results will be reported later.

REFERENCES

[1] V. Ntziachristos, J. Ripoll, L.V. Wang, and R. Weissleder. The QR Transformation I, *Nature Biotechnology*, vol. 23, no. 3, pp. 313-320, March 2005.

[2] C.H. Contag, and M.H. Bachmann. Advances in bioluminescence imaging of gene expression. *Annual Review of Biomedical Engineering*, vol. 4, pp. 235-260, 2002.

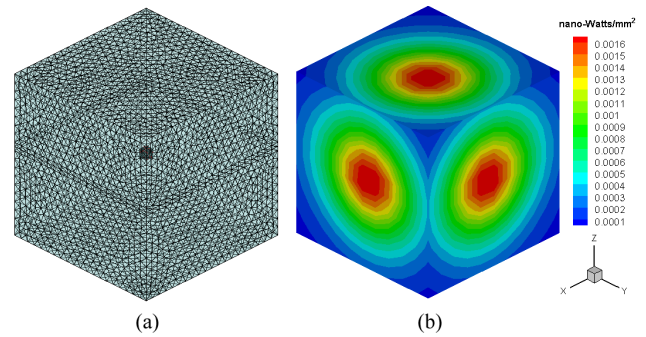


Fig. 5. (a) The volumetric mesh used in FEM simulation; (b) The photon flux density on the phantom surface calculated by FEM.

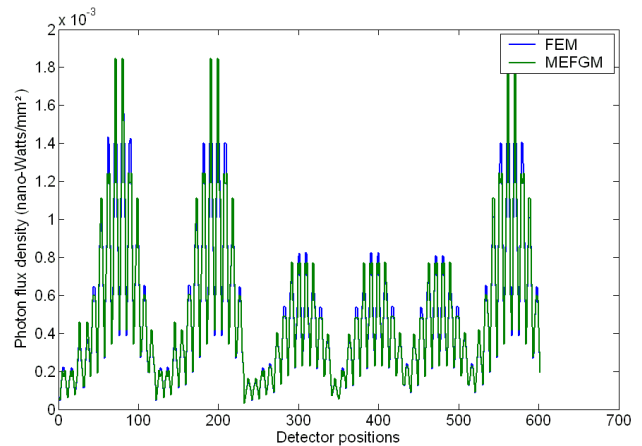


Fig. 6. Comparison of two computational results by MEFGM and FEM.

[3] W. Cong, G. Wang, D. Kumar, Y. Liu, M. Jiang, L.V. Wang, E.A. Hoffman, G. McLennan, P.B. McCray, J. Zabner, and A. Cong. Practical reconstruction method for bioluminescence tomography. *Optics Express*, vol. 13, no. 18, pp. 6765-6771, August 2005.

[4] Y. Lv, J. Tian, W. Cong, G. Wang, J. Luo, W. Yang, and H. Li. A multilevel adaptive finite element algorithm for bioluminescence tomography. *Optics Express*, vol. 14, no. 18, pp. 8211-8223, September 2006.

[5] A. P. Gibson, J. C. Hebden, S. R. Arridge. Recent advances in diffuse optical imaging. *Physics in Medicine and Biology*, vol. 50, no. 4, pp. 519-561, February 2005.

[6] J. Dolbow, and T. Belytschko. An Introduction to Programming the Meshless Element Free Galerkin Method. *Archives of Computational Methods in Engineering*, vol. 5, no. 3, pp. 207-241, July 1998.

[7] T. Belytschko, Y. Y. Lu, and L. Gu. Element-free Galerkin method. *International Journal for Numerical Methods in Engineering*, vol. 37, no. 2, pp. 229-256, June 1994.

[8] T. Belytschko, L. Gu, and Y. Y. Lu. Fracture and crack growth by element-free Galerkin methods. *Modelling and Simulation in Materials Science and Engineering*, vol. 2, no. 3A, pp. 519-534, 1994.

[9] S. R. Arridge, M. Schweiger, M. Hiraoka, and D. T. Delpy. A finite element approach for modeling photon transport in tissue. *Medical Physics*, vol. 20, no. 2, pp. 299-309, March/April 1993.

[10] M. Schweiger, S. R. Arridge, M. Hiraoka, and D. T. Delpy. The finite element method for the propagation of light in scattering media: Boundary and source conditions. *Medical Physics*, vol. 22, no. 11, pp. 1779-1792, November 1995.

[11] Y. Lv, J. Tian, W. Cong, W. Yang, C. Qin, and M. Xu. Spectrally resolved bioluminescence tomography with adaptive finite element: methodology and simulation. *Physics in Medicine and Biology*, vol. 52, no. 15, pp. 4497-4512, July 2007.